

# Combined Pilot-Aided and Decision-Directed Carrier Synchronization for Filtered Multitone Wireless Systems

Giulio Dainelli, Marco Moretti, Vincenzo Lottici, and Ruggero Reggiannini

## Abstract

This paper focuses on the issue of carrier frequency synchronization for filtered multitone wireless transmission over time-frequency selective fading channels. Rather than either relying only on known pilot symbols multiplexed within the transmitted burst or exploiting the specific signal structure in a blind mode, the estimation algorithm we pursue is derived from the maximum likelihood principle and takes advantage of both pilot symbols and also the unknown information-bearing symbols through specific differential decision-directed processing. When compared to conventional pilot-based methods, the proposed approach improves the frequency acquisition range without degrading estimation accuracy at even lower cost in terms of computational complexity.

## Index Terms

Filter bank multicarrier modulation, carrier frequency synchronization, time-frequency selective channels, differential decision-directed processing.

## I. INTRODUCTION

In view of their appealing features, multicarrier (MC) techniques are currently recognized as the key technology in the area of high-data-rate transmissions over fading wireless channels [1]. The interest surrounding MC schemes is demonstrated by their adoption in several standards,

The authors are with the Department of Information Engineering, University of Pisa, I-56122 Pisa, Italy.

Parts of this work have been presented at 8<sup>th</sup> International Workshop on Multi-Carrier Systems & Solutions (MC-SS), May 2011.

Email: [marco.moretti@iet.unipi.it](mailto:marco.moretti@iet.unipi.it)

either in the form of orthogonal frequency division multiplexing (OFDM) modulation, as in terrestrial digital audio broadcasting (DAB) and video broadcasting (DVB-T/H) [2], IEEE 802.11 Wi-Fi indoor wireless LANs [3], IEEE 802.16 Wi-Max broadband wireless access (BWA) [4] and 3GPP Long Term Evolution (LTE) [5], or based on filter bank MC (FBMC) modulation, as in the return channel of terrestrial DVB (DVB-RCT) [6] and the release 2 of the ETSI terrestrial trunked radio (TETRA) enhanced data system (TEDS) air interface [7]-[8]. The advantages of MC signaling have to be necessarily traded off, however, against a considerable sensitivity to residual carrier frequency offsets (CFOs) arising from oscillator instability and Doppler effects, that have to be accurately removed from the received waveform prior to data decoding.

***Relations with Prior Works.*** In the following, for simplicity we limit our focus on the FBMC format based on a set of contiguous non-overlapping subcarriers, also referred to as filtered multitone (FMT) modulation in very high-speed digital subscriber lines (VDSL) applications (basic references are [9], [10] and the works cited therein), even though the algorithms we discuss could be adapted to different FBMC schemes, such as discrete wavelet multitone (DWMT) [11] and staggered OFDM/OQAM [12]. In the FBMC context, the algorithms proposed in the literature for CFO recovery can be classified either as pilot-aided (PA) [13]-[14] or blind [15]-[16], depending on whether they rely or not on known pilot symbols multiplexed within the transmitted burst. Most of the algorithms cited above, however, such as those in [14]-[16], are derived assuming time-invariant fading and therefore their performance gets rapidly poor whenever the channel has a significant time selectivity, as it may easily occur in wireless mobile communications. Conversely, the PA-based maximum-likelihood estimator (PA-MLE) recently proposed in [13] efficiently copes with time-frequency selective channels assuming statistical knowledge of the channel in terms of fading covariance matrix.

***Purpose and contributions.*** The PA-MLE approach shows better estimation accuracy as compared to blind algorithms [15]-[16] in spite of substantially lower computational requirements. However, the interval of frequency offsets where it offers reliable performance, the so-called *acquisition range*, is given approximately by the inverse of the time-domain pilot spacing, and consequently, it may turn out to be very narrow as pilot symbols cannot be packed too tightly within the burst not to degrade spectrum and power efficiency. This strong limitation motivates our search for an improved version of the PA-based CFO estimator capable of extended acquisition range while retaining good accuracy and affordable complexity. Compared to previous

schemes, the proposed novel estimation approach exhibits several distinctive features, as outlined in the following:

- 1) We exploit (known) pilot symbols as in [13] but, as a further step ahead, we also take advantage of the presence of the (unknown) information-bearing symbols through a specific (non-linear) differential decision-directed (DD) based processing. In our view, combining together the PA and DD concepts for CFO recovery represents a major point of novelty. Indeed, to our knowledge, the combined PA-DD approach has received much less consideration in synchronization than that obtained in other contexts, as for instance in iterative soft or hard channel estimation.
- 2) Modulation symbols are supposed to belong to a 4-QAM constellation, an assumption that may appear at first glance too restrictive. However, we recall that 4-QAM is often adopted when frequency acquisition is being carried out in the receiver startup process. This occurs in the TETRA 2 standard [7]-[8], for instance, wherein 4-, 16- and 64-QAM formats are employed during data transmission, but a specific mixed pilot/data frequency correction burst made of all 4-QAM symbols is used for initial receiver frequency recovery.
- 3) The rationale behind our approach combining the PA and DD concepts together is as follows: *i)* we start from the log-likelihood function (LLF) for the joint estimation of the CFO and data symbols; *ii)* we get rid of data symbols in the LLF replacing them by differential decisions drawn on pairs of received samples taken on the subcarriers, without requiring any prior knowledge of either the CFO or the channel gains; *iii)* to save complexity we approximate the fading covariance matrix by a block-diagonal structure and optimize the resulting simplified metric.
- 4) Simulation runs in typical mobile wireless scenarios confirm that the proposed CFO recovery algorithm, when compared to conventional PA-MLE offers a wider acquisition range with an improvement or no degradation in estimation accuracy, at even lower complexity.

**Organization.** Sect. II describes the FMT signal model, while Sect. III first reviews the PA-MLE CFO synchronization issues, and then illustrates the proposed PA-DD algorithm. The computational complexity of the algorithm is analyzed and evaluated in Sect. IV. Sect. V presents and discusses simulation results. Finally, conclusions are drawn in Sect. VI.

**Notations.** Matrices are in uppercase bold while column vectors are in lowercase bold,  $(\cdot)^T$  denotes transpose,  $(\cdot)^H$  denotes conjugate transpose,  $(\cdot)^{-1}$  denotes inverse,  $[\mathbf{A}]_{i,j}$  denotes the  $(i, j)$  entry of the matrix  $\mathbf{A}$ ,  $\text{tr}\{\mathbf{A}\}$  denotes the trace of the matrix  $\mathbf{A}$ ,  $\|\mathbf{A}\|$  denotes the 2-norm of the matrix  $\mathbf{A}$ ,  $\text{diag}(\cdot)$  converts a sequence of size  $N$  into a  $N \times N$  diagonal matrix,  $\text{Diag}(\cdot)$  converts a sequence of  $N$  matrices of size  $L \times L$  into a  $NL \times NL$  block-diagonal matrix,  $\mathbf{I}_N$  is the  $N \times N$  identity matrix,  $\otimes$  denotes convolution,  $\mathbf{T}\{\cdot\}$  denotes the 4-QAM hard threshold detector,  $J_0(\cdot)$  denotes the first-type Bessel function of order 0, and  $\mathbb{E}\{\cdot\}$  denotes statistical expectation.

## II. FMT SIGNAL MODEL

In a FMT communication system, the available bandwidth is split into a set of  $N$  adjacent non-overlapping subcarriers [10], each of which is shaped by means of a square root raised cosine (SRRC) prototype filter having impulse response  $g(t)$  with roll-off factor  $\xi$  and frequency-shifted at multiples of  $(1+\xi)/T$ ,  $T$  being the subcarrier signaling interval; see the block diagram of Fig. 1 as a reference. Denoting with  $a_l^{(q)}$  the information or pilot symbol transmitted over the  $q$ -th subcarrier,  $0 \leq q \leq N-1$ , within the  $l$ -th FMT block,  $0 \leq l \leq L-1$ , and constraining the quantity  $M \triangleq (1+\xi)N$  to be an integer for ease of implementation, the FMT signal transmitted over a burst of  $L$  consecutive blocks can be written as

$$s(t) = \sum_{l=0}^{L-1} \sum_{q=0}^{N-1} a_l^{(q)} g(t - lT) e^{j2\pi qMt/NT}. \quad (1)$$

Differently from [14]-[16] and following the approach in [13], we assume that the propagation channel is *selective* both in time and frequency, with impulse response given by  $c(t) = \sum_{u=0}^{U-1} \rho_u(t) \delta(t - \tau_u)$ , where  $U$  is the total number of paths, while  $\rho_u(t)$  and  $\tau_u$  are the time-varying complex gains and the delays of the  $u$ -th path, respectively. At the receiver side, the input waveform  $x(t) \triangleq s(t) \otimes c(t)$  is sampled at rate  $M/T$ , processed by the cascade of the receiver polyphase filter bank (that performs matched filtering on each subcarrier) and the DFT unit, as shown in the lower part of Fig. 1. As last step, data detection is performed after channel equalization. Assuming error-free timing recovery, it can be shown under some mild assumptions that the sample taken on the  $n$ -th subcarrier at the instant  $t = kT$  at the output of the DFT unit can be accurately approximated as [13]

$$z_k^{(n)} \simeq \varphi_k^{(n)} a_k^{(n)} e^{j2\pi\nu k} + w_k^{(n)}, \quad (2)$$

where

$$\varphi_k^{(n)} \triangleq e^{j\vartheta} \sum_{u=0}^{U-1} \rho_u(kT) e^{-j2\pi n M \tau_u / NT} \quad (3)$$

is a multiplicative factor correlated both in time and frequency accounting for the channel selectivity,  $\nu$  is the CFO normalized to the signaling rate  $1/T$ ,  $\vartheta$  is the phase offset, and  $w_k^{(n)}$  is a complex-valued zero-mean independent Gaussian random variable (RV) with variance  $\sigma^2 = 2N_0$ . We remark that  $a_k^{(n)}$  in (2) corresponds to a known pilot symbol for the pair of indexes  $n$  and  $k$  such that  $n \in \mathcal{N}$  and  $k \in \mathcal{K}$ .

Letting  $\mathbf{z}^{(n)} \triangleq [z_0^{(n)}, \dots, z_{L-1}^{(n)}]^T$ ,  $\boldsymbol{\varphi}^{(n)} \triangleq [\varphi_0^{(n)}, \dots, \varphi_{L-1}^{(n)}]^T$  and  $\mathbf{w}^{(n)} \triangleq [w_0^{(n)}, \dots, w_{L-1}^{(n)}]^T$  denote the vectors collecting the received samples at the DFT output, the time-varying channel gains and the noise samples, respectively, on the  $n$ -th subcarrier, from (2) it follows that

$$\mathbf{z}^{(n)} = \boldsymbol{\Psi}(\nu) \mathbf{A}^{(n)} \boldsymbol{\varphi}^{(n)} + \mathbf{w}^{(n)}, \quad (4)$$

where  $\boldsymbol{\Psi}(\nu)$  and  $\mathbf{A}^{(n)}$  are  $L \times L$  diagonal matrices defined as  $\boldsymbol{\Psi}(\nu) \triangleq \text{diag} \{1, e^{j2\pi\nu}, \dots, e^{j2\pi\nu(L-1)}\}$  and  $\mathbf{A}^{(n)} \triangleq \text{diag} \{a_0^{(n)}, \dots, a_{L-1}^{(n)}\}$ . Hence, stacking  $\mathbf{z}^{(n)}$ ,  $\boldsymbol{\varphi}^{(n)}$  and  $\mathbf{w}^{(n)}$  to form  $\mathbf{z} \triangleq [\mathbf{z}^{(0)T}, \dots, \mathbf{z}^{(N-1)T}]^T$ ,  $\boldsymbol{\varphi} \triangleq [\boldsymbol{\varphi}^{(0)T}, \dots, \boldsymbol{\varphi}^{(N-1)T}]^T$  and  $\mathbf{w} \triangleq [\mathbf{w}^{(0)T}, \dots, \mathbf{w}^{(N-1)T}]^T$ , the observed sequence can be expressed as

$$\mathbf{z} = \boldsymbol{\Gamma}(\nu) \mathbf{A} \boldsymbol{\varphi} + \mathbf{w}, \quad (5)$$

where  $\boldsymbol{\Gamma}(\nu)$  and  $\mathbf{A}$  are  $LN \times LN$  diagonal matrices defined as  $\boldsymbol{\Gamma}(\nu) \triangleq \text{Diag} \{\boldsymbol{\Psi}(\nu), \dots, \boldsymbol{\Psi}(\nu)\}$  and  $\mathbf{A} \triangleq \text{Diag} \{\mathbf{A}^{(0)}, \dots, \mathbf{A}^{(N-1)}\}$ .

### III. ML CARRIER FREQUENCY ESTIMATION

#### A. Formulation of the ML Estimation Problem

Let us model the set of channel coefficients  $\boldsymbol{\varphi}$  as a complex zero-mean Gaussian random vector with covariance matrix  $\mathbf{C}_\varphi \triangleq E\{\boldsymbol{\varphi}\boldsymbol{\varphi}^H\}$ . We note that since  $\mathbf{C}_\varphi$  changes slowly with time, it can be estimated at the receiver either through channel sounding or exploiting the a-priori knowledge about the multipath delay profile and the Doppler spread. For later use, in Appendix A  $\mathbf{C}_\varphi$  is calculated under the assumptions that the path delays are either independent exponentially-distributed RVs or deterministic parameters.

Given the CFO  $\nu$  and the matrix  $\mathbf{A}$  collecting all the symbols transmitted within the burst, it turns out that the received samples  $\mathbf{z}$  in (5) are jointly complex zero-mean Gaussian as well,

with covariance matrix

$$\mathbf{C}_z(\nu) \triangleq E\{\mathbf{z}\mathbf{z}^H\} = \mathbf{\Gamma}(\nu)\mathbf{A}\mathbf{C}_\varphi\mathbf{A}^H\mathbf{\Gamma}(\nu)^H + \sigma^2\mathbf{I}_{LN}. \quad (6)$$

In light of (6), the joint ML estimate (JMLE) of the normalized CFO and the transmitted symbols is obtained by maximizing the LLF as

$$(\hat{\nu}, \hat{\mathbf{A}}) = \underset{\tilde{\nu} \in \mathcal{I}, \tilde{\mathbf{A}} \in \mathcal{A}}{\operatorname{argmin}} \{ \Lambda_{\text{JMLE}}(\tilde{\nu}, \tilde{\mathbf{A}}) \}, \quad (7)$$

where the JMLE metric reads as

$$\Lambda_{\text{JMLE}}(\nu, \mathbf{A}) \triangleq \mathbf{z}^H \mathbf{\Gamma}(\nu) \mathbf{A} \mathbf{F} \mathbf{A}^H \mathbf{\Gamma}(\nu)^H \mathbf{z}, \quad (8)$$

where  $\mathbf{F} \triangleq (\mathbf{C}_\varphi + \sigma^2\mathbf{I}_{LN})^{-1}$ , while the interval  $\mathcal{I}$  includes the possible trial values for  $\nu$  and  $\mathcal{A}$  is the set of all possible realizations of the transmitted symbol matrix  $\mathbf{A}$ . Finding the JMLE requires solving a mixed integer optimization problem involving a multidimensional search over the sets  $\mathcal{I}$  and  $\mathcal{A}$ . Due to its combinatorial nature, however, the computational complexity of (7) becomes intractable even for small  $L$  and  $N$ , and consequently, alternative methods for efficient CFO recovery need to be devised.

A good complexity-vs-accuracy tradeoff is offered by the PA-MLE approach pursued in [13]. Therein, the main assumption is that each of  $S$  subcarriers, with  $S \leq N$ , conveys  $P$  pilot symbols, with  $P \leq L$ , so that the total number of known pilots embedded in the transmitted burst amounts to  $Q \triangleq PS$ . Exploiting the fact that observation model (5) still holds when applied to the subset of received samples corresponding to pilot positions (with the only difference that  $\mathbf{z}$ ,  $\varphi$  and  $\mathbf{w}$  are now  $Q$ -dimensional vectors and  $\mathbf{\Gamma}(\nu)$ ,  $\mathbf{A}$  and  $\mathbf{C}_\varphi$  are  $Q \times Q$  diagonal matrices, with  $Q < LN$ ), we can build a metric quite similar to that in (8), which no longer depends on the (unknown) data symbols but only on the frequency offset to be estimated; see [13] for additional details. The following remarks about the PA-MLE method can be of help.

- 1) Since the matrix inversion to obtain  $\mathbf{F}$  for a given  $\mathbf{C}_\varphi$  and  $\sigma^2$  required by the metric (8) can be performed off-line, the PA-MLE can be obtained through a two-step procedure based on a linear grid search over the interval  $\mathcal{I}$  of trial values  $\tilde{\nu}$  (coarse search), which can be efficiently carried out using FFT, followed by interpolation (fine search) [13].
- 2) For sake of simplicity, it is appropriate to remove the dependence of  $\mathbf{F}$  on  $\sigma$ , i.e., on the received signal-to-noise-ratio (SNR), by setting it to a predefined value  $\sigma_0$ ; see Sect. V-A for further details about this issue.

- 3) It can be argued that the acquisition range of the PA-MLE gets larger by reducing the pilot spacing in the time-domain, i.e., by increasing the number of pilot symbols  $Q$  within the time-frequency grid. It is also true, however, that the pilot overhead  $\chi \triangleq \frac{Q}{NL}$  has to be chosen as low as possible, say below 10%, not to degrade power and spectrum efficiency.

### B. Combined Pilot-Aided and Decision-Directed Frequency Estimation

The contrasting requirements about the choice of  $Q$  discussed above motivate the search for a more efficient alternative to the PA-MLE scheme. Rather than increasing the number of pilots  $Q$ , thereby incurring an efficiency loss, we pursue a different estimation strategy based on combining the PA and DD concepts together, an approach referred to in the sequel as combined MLE (CMLE). In a nutshell, the idea is not only to exploit the known pilot symbols, but also the unknown information-bearing data via some form of hard DD-based processing. The main steps of the CMLE approach can be summarized as follows.

- 1) The metric  $\Lambda_{\text{JMLE}}(\nu, \mathbf{A})$  in (8) can be reformulated after some algebra into

$$\Lambda_{\text{JMLE}}(\nu, \mathbf{A}) = \sum_{l=0}^{L-1} \sum_{s,c=0}^{N-1} a_l^{(s)} a_l^{(c)*} z_l^{(s)*} z_l^{(c)} G_{l,l}^{(s,c)} + 2 \sum_{k=1}^{L-1} \sum_{l=0}^{L-1-k} \text{Re} \left\{ e^{-j2\pi\nu k} \sum_{s,c=0}^{N-1} a_l^{(s)} a_{l+k}^{(c)*} z_l^{(s)*} z_{l+k}^{(c)} G_{l,l+k}^{(s,c)} \right\}, \quad (9)$$

where  $G_{n,m}^{(s,c)} \triangleq [\mathbf{G}]_{(s-1)L+n, (c-1)L+m}$ , with  $\mathbf{G}$  being defined as  $\mathbf{G} \triangleq (\mathbf{C}_\varphi + \sigma_0^2 \mathbf{I}_{LN})^{-1}$ , i.e., the matrix  $\mathbf{F}$  in (8) evaluated at  $\sigma = \sigma_0$ .

- 2) The metric (9) depends on all the products between any two symbols (data or pilots) within the burst. This basic fact suggests that a possible way of getting rid of the unknown data symbols is to resort to the differential decisions taken on the products  $z_l^{(s)} z_{l+k}^{(c)*}$ . From (2), indeed, it can be easily obtained

$$z_l^{(s)} z_{l+k}^{(c)*} = \varphi_l^{(s)} \varphi_{l+k}^{(c)*} a_l^{(s)} a_{l+k}^{(c)*} e^{-j2\pi\nu k} + \zeta_{l,l+k}^{(s,c)}, \quad (10)$$

where  $\zeta_{l,l+k}^{(s,c)}$  is a disturbance term accounting for both channel noise and fading. Now, we invoke the following restrictive assumptions, the first two of which are provisional and will be shortly dropped, while the third one is not limiting in view of the discussion made in point 2) of Sect. I.

- A1) The channel fading is sufficiently correlated in both time- and frequency domains so that  $\varphi_l^{(s)}\varphi_{l+k}^{(c)*} \simeq \left|\varphi_l^{(s)}\right|^2$  holds, regardless of the time lag  $k$ ,  $1 \leq k \leq L - 1$ , and the subcarrier index difference  $|s - c|$ ,  $0 \leq s, c \leq N - 1$ .
- A2) The normalized CFO  $\nu$  is sufficiently small so that  $e^{-j2\pi\nu k} \simeq 1$ , for  $0 \leq k \leq L - 1$ .
- A3) The data and pilot symbols belong to a 4-QAM constellation with unitary radius, and all pilots are equal.
- 3) After defining the *differential symbol*  $b_{l,l+k}^{(s,c)} \triangleq a_l^{(s)} a_{l+k}^{(c)*}$ , applying A1)-A2) in (10) yields

$$z_l^{(s)} z_{l+k}^{(c)*} \simeq \left|\varphi_l^{(s)}\right|^2 b_{l,l+k}^{(s,c)} + \zeta_{l,l+k}^{(s,c)}. \quad (11)$$

Hence, in view of A3), the differential symbol  $b_{l,l+k}^{(s,c)}$  belongs to a 4-QAM constellation as well, and due to (11) can be estimated without the knowledge of both the CFO and the channel gains, by feeding the product  $z_l^{(s)} z_{l+k}^{(c)*}$  into a conventional 4-QAM hard threshold detector, i.e.,

$$\hat{b}_{l,l+k}^{(s,c)} = \mathbf{T} \left\{ z_l^{(s)} z_{l+k}^{(c)*} \right\}. \quad (12)$$

- 4) Now, we show that assumptions A1) and A2) can be properly relaxed. First, we observe that due to A3) the differential symbol  $b_{l,l+k}^{(s,c)}$  can be written as the product of a sequence of differential symbols, each involving either adjacent symbols on the same subcarrier (in the time domain) or symbols over different subcarriers with the same time index (in the frequency domain). For instance, letting  $s > c$  and exploiting  $a_l^{(s)} a_l^{(s)*} = 1$ , one gets

$$\begin{aligned} b_{l,l+k}^{(s,c)} &= a_l^{(s)} a_{l+1}^{(s)*} a_{l+1}^{(s)} \cdots a_{l+k}^{(s)*} a_{l+k}^{(s)} a_{l+k}^{(s-1)*} a_{l+k}^{(s-1)} \cdots a_{l+k}^{(c+1)*} a_{l+k}^{(c+1)} a_{l+k}^{(c)*} \\ &= b_{l,l+1}^{(s,s)} \cdots b_{l+k,l+k}^{(c+1,c)}. \end{aligned} \quad (13)$$

The result in (13) suggests that the detection of  $b_{l,l+k}^{(s,c)}$  can be carried out by means of concatenated decisions on the differential symbols corresponding to data symbols placed contiguously either in time or frequency, so that these decisions are minimally affected by both the channel fading and the CFO. On the other hand, each differential decision may be in error mainly due to noise, and also possibly by fading and the CFO. So, the number of intermediate steps in (13) should be kept as small as possible. Our idea is then to also exploit the known pilot symbols as follows. Let us designate as  $p_{\bar{l}}^{(\bar{s})}$  and  $p_{\bar{q}}^{(\bar{c})}$  the pilots closest to the data symbols  $a_l^{(s)}$  and  $a_{l+k}^{(c)}$ , respectively, in the time-frequency grid. We note that there are pilot symbols close to any data symbol insofar as the pilot pattern has to be

employed for channel estimation as well, and accordingly, it has to be designed such that the fading process is tightly sampled on both time and frequency domains. Hence, taking into account in view of A3) that  $p_{\bar{l}}^{(s)*} p_{\bar{q}}^{(c)} = 1$ , the differential symbol can be rearranged as

$$b_{l,q}^{(s,c)} = a_l^{(s)} p_{\bar{l}}^{(s)*} p_{\bar{q}}^{(c)} a_q^{(c)*} = b_{l,\bar{l}}^{(s,\bar{s})} b_{\bar{q},q}^{(\bar{c},c)}. \quad (14)$$

and therefore, it can be detected through the product of decisions

$$\hat{b}_{l,q}^{(s,c)} = \hat{b}_{l,\bar{l}}^{(s,\bar{s})} \hat{b}_{\bar{q},q}^{(\bar{c},c)}, \quad (15)$$

where each differential decision is taken on closely spaced samples, with the result that error propagation is strongly mitigated. Collecting all the above together, we can conclude that:

- assumption A1) can be substantially dropped, as for the algorithm to work correctly it is sufficient that there exists significant fading correlation only between *adjacent* symbols both along time and frequency;
  - assumption A2) can be replaced by the far milder condition that the phase rotation induced by the CFO is negligible in a *single* symbol interval only.
- 5) Thus, replacing the product  $a_l^{(s)} a_{l+k}^{(c)*}$  in (9) by the differential decision  $\hat{b}_{l,l+k}^{(s,c)}$  computed through (15), and dropping immaterial factors independent of the CFO, the CMLE metric can be written as

$$\Gamma_{\text{CMLE}}(\nu) = \sum_{k=1}^{L-1} \sum_{l=0}^{L-1-k} \text{Re} \left\{ e^{-j2\pi\nu k} \sum_{s,c=0}^{N-1} \hat{b}_{l,l+k}^{(s,c)} z_l^{(s)*} z_{l+k}^{(c)} G_{l,l+k}^{(s,c)} \right\}, \quad (16)$$

whose minimization provides the CMLE solution.

#### IV. COMPUTATIONAL COMPLEXITY ISSUES

We now focus on some issues concerning the computational complexity of the CMLE-based CFO recovery.

- 1) Compared to (9), the CMLE metric in (16) does no longer depend on the unknown data symbols, since they have been replaced by the differential decisions (12) taken on the products  $z_l^{(s)} z_{l+k}^{(c)*}$ . Therefore, the CMLE requires the same two-step search procedure on the interval  $\mathcal{I}$  we already mentioned for the PA-MLE in Sect. III-A.

- 2) Let us observe that due to the specific way the fading vector  $\varphi$  is built, the covariance  $\mathbf{C}_\varphi$  is a block-Toeplitz matrix composed of  $N^2$  sub-matrices  $\mathbf{C}_\varphi^{(n,m)}$ ,  $1 \leq n, m \leq N$ , of size  $L \times L$ , each representing the covariance between the subcarriers of indexes  $n$  and  $m$ . Hence, a possible route to further simplify the CMLE algorithm consists of ignoring the correlation between the fading coefficients belonging to different subcarriers, i.e., replacing  $\mathbf{C}_\varphi$  by  $\bar{\mathbf{C}}_\varphi \triangleq \text{Diag} \left\{ \mathbf{C}_\varphi^{(1,1)}, \dots, \mathbf{C}_\varphi^{(N,N)} \right\}$ . As a consequence, the simplified CMLE employing the covariance  $\bar{\mathbf{C}}_\varphi$  is actually mismatched to the actual fading conditions, although the resulting performance loss is moderate, as proved by the simulation results in Sect. V. Further, thanks to the stationarity of channel fading, we have  $\bar{\mathbf{\Omega}} \triangleq \mathbf{C}_\varphi^{(1,1)} = \mathbf{C}_\varphi^{(2,2)} = \dots = \mathbf{C}_\varphi^{(N,N)}$ , and therefore,  $\bar{\mathbf{C}}_\varphi = \text{Diag} \left\{ \bar{\mathbf{\Omega}}, \dots, \bar{\mathbf{\Omega}} \right\}$ . As a result, the inverse  $\bar{\mathbf{G}} \triangleq \left( \bar{\mathbf{C}}_\varphi + \sigma_0^2 \mathbf{I}_{LN} \right)^{-1}$  can be computed as a block diagonal matrix whose blocks are all equal to the  $L \times L$  matrix  $\bar{\mathbf{\Delta}} \triangleq \left( \bar{\mathbf{\Omega}} + \sigma_0^2 \mathbf{I}_L \right)^{-1}$ . Accordingly, the CFO recovery algorithm employing  $\bar{\mathbf{G}}$  instead of  $\mathbf{G}$  in (16) will be designated as low-complexity CMLE, or LC-CMLE for short, and the relevant metric to be minimized will be expressed as

$$\Phi_{\text{LC-CMLE}}(\nu) = \sum_{k=1}^{L-1} \sum_{l=0}^{L-1-k} \text{Re} \left\{ e^{-j2\pi\nu k} \Delta_{l,l+k} \sum_{s=0}^{N-1} \hat{b}_{l,l+k}^{(s,s)} z_l^{(s)*} z_{l+k}^{(s)} \right\}, \quad (17)$$

where  $\Delta_{l,l+k} \triangleq [\bar{\mathbf{\Delta}}]_{l,l+k}$ .

- 3) To evaluate the complexity of the CFO recovery schemes illustrated so far, we adopt the following assumptions:
- A4) the computational complexity load is defined as the number of real-valued floating point operations, i.e., additions and multiplications, referred to in the following as real-flops for short, required to compute the metric to be optimized at the  $N_\nu$  (equi-spaced) trial values within the search interval  $\mathcal{I}$ ;
  - A5) given  $\mathbf{C}_\varphi$  and  $\sigma_0$ , the matrix  $\mathbf{G}$  for the PA-MLE is computed only once as product between an upper and lower triangular matrices via Cholesky decomposition;
  - A6) the multiplications involved by the differential decisions are not taken into account as they correspond to phase rotations by multiples of  $\pi/2$ , and can be easily performed by swapping the real and/or imaginary parts of the operands;
  - A7) the values of  $e^{-j2\pi\nu k}$  at the  $N_\nu$  trial values in  $\mathcal{I}$  are stored in a look-up table;
  - A8) the parameters  $N$ ,  $L$  and  $N_\nu$  are assumed to be of the same order of magnitude.

Hence, from the analysis detailed in Appendix B we end up to the results summarized in Tab. I. It is seen that the LC-CMLE shows a complexity order reduced by  $N$  when compared to the CMLE and, in view of A8), lower than that of the PA-MLE.

## V. PERFORMANCE RESULTS

In this section, simulations results over doubly-selective fading scenarios are employed to compare the accuracy of the PA-MLE, CMLE and LC-CMLE schemes. Two performance benchmarks are considered: *i*) the PA-MLE scheme with  $Q = NL$  pilots, i.e., where all the burst symbols are assumed to be known, which will be referred to as data-aided MLE (DA-MLE), and *ii*) the corresponding Cramer-Rao lower bound (CRLB), derived in Appendix C. First, we focus on the mean square estimation error (MSEE) defined as  $E\{(\hat{\nu} - \nu)^2\}$  as a function of the true normalized CFO  $\nu$  for a given received mean-energy-per-symbol-to-noise-spectral-density ratio  $E_s/N_0$ , that permits to identify the *acquisition range* of the CFO estimation algorithm. Next, the *noise sensitivity* is assessed in terms of the MSEE as a function of  $E_s/N_0$  for a specified CFO to be estimated.

### A. Simulation Setup

The selection of signal and channel parameters employed in simulations can be considered as typical in mobile radio applications, such as e.g. in [8]. Each burst is composed of  $N$  subcarriers, with  $N = 16, 32, 64, 128$ , and spans  $L = 51$  FMT symbol intervals. A uniform pilot pattern is chosen with  $S = N/2$  subcarriers, each bearing  $P = 6$  pilots, so that the total number is  $Q = PS = 3N$ , and the pilot overhead is  $\chi \simeq 6\%$ , regardless the value of  $N$ . For instance, the pilot distribution we adopted for  $N = 16$  subcarriers is such that the pilot symbol transmitted over the  $n$ -th subcarrier within the  $k$ -th FMT block is identified by  $n \in \mathcal{N} = \{0, 2, 4, 6, 9, 11, 13, 15\}$  and  $k \in \mathcal{K} = \{0, 9, 19, 29, 39, 49\}$ , with  $Q = 48$ . The roll-off factor of the SRRC prototype filter  $g(t)$  is set to  $\xi = 0.25$ , while both data and pilot symbols are unit-energy 4-QAM symbols.

The channel is time- and frequency-selective with  $U = 6$  paths. As usually assumed in FMT wireless transmissions over selective fading channels, the path delays  $\tau_u$ ,  $0 \leq u \leq U - 1$ , are chosen to be uniformly spaced (with  $\tau_0 = 0$  for simplicity), whereas the path gains are modeled as zero-mean independent complex-valued Gaussian processes, having Jakes power spectrum with Doppler bandwidth  $f_D$  and variance decaying exponentially with  $\tau_u$ , adjusted so that the

normalized channel delay spread is  $\sigma_\tau/T = 2 \cdot 10^{-2}$ . Two different propagation environments are considered: slow-fading (SF) with  $f_D T = 7.5 \cdot 10^{-3}$  and fast-fading (FF) with  $f_D T = 3 \cdot 10^{-2}$ . As an example, in Fig. 2 we show a realization of the time-frequency fading process affecting the transmitted burst for the FF scenario and  $N = 16$  subcarriers. It is apparent that our choice of time and Doppler spread leads to severe doubly-selective fading conditions along both time and frequency.

Further, concerning the noise variance  $\sigma_0^2$  adopted by the estimators in the matrices  $\mathbf{G}$  (PA-MLE and CMLE) and  $\mathbf{\Delta}$  (LC-CMLE), its value is selected so that the corresponding  $E_s/N_0$  is equal to 15 dB. The reason behind this choice is twofold. First, it comes from the observation (resulting from intensive simulation trials) that the above value safely avoids the numerical instability inherent in the matrix inversion involved in the definition of  $\mathbf{G}$  and  $\mathbf{\Delta}$ . On the other side,  $\sigma_0^2$  has not to be too small so that  $\mathbf{G}$  and  $\mathbf{\Delta}$  can be still considered approximately “matched” to the receiver operating point, i.e., its sensitivity, although some performance loss may arise at higher SNRs.

### B. Complexity Comparison

To compare the complexity load of the CFO recovery schemes discussed so far, we focus on the setup outlined in Sect. V-A and assume two test cases based on  $N = 16$  and  $N = 128$  subcarriers, letting the number of CFO trial values be  $N_\nu = 30$ . Denoting as  $\mathcal{C}_{\text{PA-MLE}}$ ,  $\mathcal{C}_{\text{CMLE}}$  and  $\mathcal{C}_{\text{LC-CMLE}}$  the number of real-flops required by the the PA-MLE, CMLE and LC-CMLE, respectively, according to the results of Appendix B, we can write

$$\mathcal{C}_{\text{PA-MLE}}/\mathcal{C}_{\text{CMLE}} \simeq N_\nu \chi^2 = 0.108, \quad (18)$$

$$\mathcal{C}_{\text{PA-MLE}}/\mathcal{C}_{\text{LC-CMLE}} \simeq 2N_\nu \chi^2 N = 0.216N. \quad (19)$$

where the conventional PA-MLE was taken as the reference benchmark. From inspection of (18)-(19) it can be concluded that *i*) the complexity of the CMLE is an order of magnitude *larger* than PA-MLE irrespective of  $N$ , and *ii*) the complexity of LC-CMLE is *smaller* by a factor linearly scaling with  $N$ , namely around 3.46 ( $N = 16$ ) and 27.7 ( $N = 128$ ).

### C. Acquisition Range

The acquisition range is shown in Figs. 3 and 4 for the SF and FF channels, respectively, assuming  $N = 16$  subcarriers and  $E_s/N_0$  of 30 dB. For both scenarios, it is worth noting that: *i*) the MSEE of the DA-MLE (in the considered interval of  $\nu$ ) turns out to be nearly independent of the CFO, and *ii*) both the LC-CMLE and CMLE outperform the PA-MLE, i.e., the latter exhibits a definitely narrower acquisition range, although all the estimators have a comparable MSEE. These results are consistent with the well-known rule that in PA-based synchronization the acquisition range is roughly as wide as the inverse of the time-domain pilot spacing; see [13] and references therein. When we arrange pilots adjacent together as in DA-MLE, indeed, the acquisition range is approximately equal to the inverse of symbol interval, i.e.,  $1/T$ , while spacing them one every 10 data symbols as in the PA-MLE gives a narrower acquisition range, i.e., around 10 % of  $1/T$ . On the other side, combining pilots and differential decisions together makes the acquisition range of both the CMLE and LC-CMLE around twice as wide as compared to the PA-MLE. Therefore, we get the interesting result that the combined PA-DD approach can considerably widen the acquisition range without having to pay any increase in pilot overhead, nor any penalty in terms of MSEE or algorithm complexity.

Figs. 5 and 6 show plots of the MSEE for the LC-CMLE as a function of the CFO for different values of  $N$ , namely  $N = 16, 32, 64, 128$ . Again, we consider both the SF and FF scenarios, and assume  $E_s/N_0$  equal to 30 dB. Inspection of the figures reveals that the acquisition range is substantially independent of  $N$ , while the MSEE floor tends to improve as  $N$  grows, in view of the larger number of observations available to the estimator.

Over the faster (FF) channel, as shown in Figs. 4 and 6, the acquisition range of all the algorithms tend to degrade if compared to the slow channel (Figs. 3 and 5), inasmuch as both the CMLE and LC-CMLE algorithms (and the PA-MLE as well) exhibit a more rounded MSEE curve about the minimum at  $\nu = 0$ . This behavior can be explained noting that the larger the Doppler bandwidth or, in other words, the less the time-domain fading correlation, the less accurate the assumption A1) in Sect. III-B even on a interval of a few symbols. A similar effect can be ascribed to a reduction of  $E_s/N_0$ , since this leads to a larger error rate in the differential decisions (12) and jointly to a higher sensitivity of the CMLE and LC-CMLE schemes to a nonzero CFO. Actually, in both cases, i.e., faster fading and larger noise, the CFO estimation

accuracy degrades due to a less reliable cancellation of the modulation phase shifts in the metrics (16) and (17). Nevertheless, the plots show that the limits of the acquisition range are hardly affected if measured at a reasonable MSEE level, say  $10^{-4}$ , and accordingly, the performance margins offered by the CMLE and LC-CMLE still hold.

It is worth noting that the availability of a wider acquisition range allows to accommodate more severe Doppler-induced frequency deviations, that are sometimes hard to recover via the more classical PA-MLE scheme. Consider for instance the TETRA Release 2 standard [7], where the carrier frequency is either 400 MHz or 800 MHz, and the signaling rate  $1/T$  is 2.4 kHz. Assuming a terminal speed of 200 km/h, the worst-case Doppler shift amounts to  $\pm 150$  Hz, which is fully covered by the acquisition range of 10% of  $1/T$ , i.e.,  $\pm 240$  Hz, featured by the CMLE and LC-CMLE algorithms, while use of PA-MLE in this case would be more troublesome.

#### D. Noise sensitivity

Figures 7 and 8 show the MSEE over the SF and FF channels, respectively, as a function of  $E_s/N_0$  assuming that the CFO to be estimated is  $\nu = 0$ . As for the SF scenario of Fig. 7, it can be noted that: *i*) the DA-MLE does not achieve the CRLB due to the finite data record [17], while the additional MSEE gap of the other estimators is due, respectively, to the limited number of pilots  $Q < NL$  transmitted within the burst (PA-MLE), to errors on differential decisions (CMLE and LC-CMLE) and to the approximation of the fading covariance matrix as a diagonal block matrix (LC-CMLE); *ii*) as expected, the CMLE closely approaches the DA-MLE at large SNRs thanks to the differential decisions getting asymptotically more and more reliable; *iii*) the LC-CMLE offers worse (asymptotical) performance with respect to the CMLE because of the inherent approximation of the fading covariance matrix, although its behavior is substantially equivalent to that of the PA-MLE.

Finally, results for the FF channel are illustrated in Fig. 8. Due to the faster channel variations from symbol to symbol, the MSEE curves of all the estimators depart slightly further from the CRLB if compared to what obtained in Fig. 7 for the SF channel. Then, coherently with Fig. 4, the reduced reliability of the differential decisions due to the faster channel makes now the CMLE and LC-CMLE incur a MSEE floor at large SNRs, comparable with that of the PA-MLE, although at low SNRs the CMLE performs closest to the DA-MLE.

## VI. CONCLUSIONS

We have addressed the basic design issues for a novel CFO recovery algorithm intended for FMT burst-mode transmissions over doubly-selective fading channels. Exploiting the fading correlation on time and frequency domains, the estimator relies on the combined use of two well-known concepts, namely, pilot symbols uniformly distributed within the burst and differential decisions taken on the received samples without requiring any prior knowledge of CFO and channel state. Numerical results obtained in typical mobile wireless environments confirm that the proposed estimation approach, when compared to the conventional PA-MLE scheme, offers a significantly wider frequency acquisition range with no accuracy degradation at even lower complexity load.

### APPENDIX A: FADING COVARIANCE MATRIX

Let us assume that the time-varying path gains  $\rho_u(t)$  are modeled as stationary zero-mean independent complex-valued Gaussian processes, having Jakes power spectrum with Doppler bandwidth  $f_D$ , or equivalently  $\mathbb{E}\{\rho_u(t)\rho_u^*(\tau)\} = \sigma_{\rho_u}^2 J_0[2\pi f_D(t - \tau)]$ , and variance  $\sigma_{\rho_u}^2$  decaying exponentially with the path delay  $\tau_u$ . Hence, according to (3), the generic entry of the fading covariance matrix  $\mathbf{C}_\varphi$  is given by

$$\begin{aligned}
 [\mathbf{C}_\varphi]_{(s-1)L+k, (c-1)L+q} &\triangleq \mathbb{E}\{\varphi_k^{(s)} \varphi_q^{(c)*}\} \\
 &= \sum_{u=0}^{U-1} \sum_{l=0}^{U-1} \mathbb{E}\{\rho_u(kT) \rho_l^*(qT)\} \mathbb{E}\{e^{-j2\pi s M \tau_u / NT} e^{j2\pi c M \tau_l / NT}\} \\
 &= \sum_{u=0}^{U-1} \mathbb{E}\{\rho_u(kT) \rho_u^*(qT)\} \mathbb{E}\{e^{-j2\pi(s-c) M \tau_u / NT}\} \\
 &= J_0[2\pi f_D(k - q)T] \sum_{u=0}^{U-1} \sigma_{\rho_u}^2 \mathbb{E}\{e^{-j2\pi(s-c) M \tau_u / NT}\}, \quad 0 \leq k, q \leq L - 1, 0 \leq s, c \leq N - 1. \quad (20)
 \end{aligned}$$

Considering the path delays  $\tau_u$  as independent exponentially-distributed RVs with parameter  $\lambda$ , we obtain

$$\mathbb{E}\{e^{-j2\pi s M \tau_u / NT}\} = \frac{1}{1 + j2\pi s \frac{M\lambda}{NT}}, \quad (21)$$

and accordingly, (20) can be rewritten as

$$[\mathbf{C}_\varphi]_{(s-1)L+k,(c-1)L+q} = \frac{J_0[2\pi f_D(k-q)T]}{1 + j2\pi(s-c)\frac{M\lambda}{NT}} \cdot \sum_{u=0}^{U-1} \sigma_{\rho_u}^2, \quad 0 \leq k, q \leq L-1, \quad 0 \leq s, c \leq N-1. \quad (22)$$

In the specific case of path delays being deterministic quantities of type  $\tau_u = u\delta$ ,  $0 \leq u \leq U-1$ , i.e., uniformly spaced within the interval  $\Delta\tau \triangleq (U-1)\delta$ , (20) turns into

$$\begin{aligned} [\mathbf{C}_\varphi]_{(s-1)L+k,(c-1)L+q} &= \sum_{u=0}^{U-1} \mathbf{E}\{\rho_u(kT)\rho_u^*(qT)\} e^{-j2\pi(s-c)M\tau_u/NT} \\ &= J_0[2\pi f_D(k-q)T] \sum_{u=0}^{U-1} \sigma_{\rho_u}^2 e^{-j2\pi(s-c)uM\delta/NT}, \quad 0 \leq k, q \leq L-1, \quad 0 \leq s, c \leq N-1. \end{aligned} \quad (23)$$

It can be pointed out that  $[\mathbf{C}_\varphi]_{(s-1)L+k,(c-1)L+q}$  in both (22) and (23) depends only on the differences  $k-q$  and  $s-c$  taken along the time and frequency domains, respectively.

## APPENDIX B: COMPLEXITY EVALUATION

Based on assumptions A4)-A8) made in Sect. IV, we evaluate here the complexity required by the PA-MLE, CMLE and LC-CMLE algorithms.

**PA-MLE.** In view of A5), let us assume that the  $Q \times Q$  matrix  $\mathbf{G}$  is decomposed off-line as  $\mathbf{G} = \mathbf{P}\mathbf{P}^H$ , where  $\mathbf{P}$  is a lower triangular matrix with strictly positive diagonal entries. The PA-MLE metric in (8) can thus be written as

$$\Lambda_{\text{PA-MLE}}(\nu) = \|(\mathbf{\Gamma}(\nu)\mathbf{A}\mathbf{P})^H \mathbf{z}\|^2, \quad (24)$$

where  $\mathbf{\Gamma}(\nu)$  and  $\mathbf{A}$  are  $Q \times Q$  matrices and  $\mathbf{z}$  is a vector of size  $Q$ . We recall that  $Q = \chi NL$  is the total number of pilots multiplexed within the burst and  $\chi$  is the pilot overhead, as discussed in Sect. III-A.

For a given CFO trial value  $\nu \in \mathcal{I}$ , the following steps to calculate (24) are required:

- Dropping the evaluation of  $\mathbf{\Gamma}(\nu)\mathbf{A}$  due to A6), the matrix  $\mathbf{U} \triangleq \mathbf{\Gamma}(\nu)\mathbf{A}\mathbf{P}$  involves  $Q^2/2$  complex-valued operations, i.e.,  $3Q^2$  real-flops.
- About  $\mathbf{y} \triangleq \mathbf{U}^H \mathbf{z}$ , the required number of real-flops is  $3Q^2$ .
- Computing  $\Lambda_{\text{PA-MLE}}(\nu) = \|\mathbf{y}\|^2$  requires  $4Q$  real-flops.

Then, the total computational load of the PA-MLE amounts to

$$\mathcal{C}_{\text{PA-MLE}} = N_\nu(6Q^2 + 4Q) = N_\nu(6\chi^2 N^2 L^2 + 4\chi NL), \quad (25)$$

or equivalently,  $\mathcal{O}(N_\nu \chi^2 N^2 L^2)$ .

**CMLE.** The metric  $\Gamma_{\text{CMLE}}(\nu)$  in (16) can be computed according to the following steps.

- The term  $v_k \triangleq \sum_{l=0}^{L-1-k} \sum_{s,c=0}^{N-1} \hat{b}_{l,l+k}^{(s,c)} z_l^{(s)*} z_{l+k}^{(c)} G_{l,l+k}^{(s,c)}$ ,  $1 \leq k \leq L-1$ , requires  $6N^2 L^2$  real-flops.
- For a given CFO trial value  $\nu \in \mathcal{I}$ , computing  $\Gamma_{\text{CMLE}}(\nu) = \text{Re} \left\{ \sum_{k=1}^{L-1} e^{-j2\pi\nu k} v_k \right\}$  requires  $3L$  real-flops.

Then, the total computational load of the CMLE amounts to

$$\mathcal{C}_{\text{CMLE}} = 3N_\nu L + 6N^2 L^2, \quad (26)$$

or equivalently,  $\mathcal{O}(N^2 L^2)$ .

**LC-CMLE.** The metric  $\Phi_{\text{LC-CMLE}}(\nu)$  in (17) can be computed according to the following steps.

- The term  $u_k \triangleq \sum_{l=0}^{L-1-k} \Delta_{l,l+k} \sum_{s=0}^{N-1} \hat{b}_{l,l+k}^{(s,s)} z_l^{(s)*} z_{l+k}^{(s)}$ ,  $1 \leq k \leq L-1$ , requires  $L^2(3N+2)$  real-flops.
- For a given CFO trial value  $\nu \in \mathcal{I}$ , computing  $\Phi_{\text{LC-CMLE}}(\nu) = \text{Re} \left\{ \sum_{k=1}^{L-1} e^{-j2\pi\nu k} u_k \right\}$  requires  $3L$  real-flops.

Then, the total computational load of the LC-CMLE amounts to

$$\mathcal{C}_{\text{LC-CMLE}} = 3N_\nu L + L^2(3N+2), \quad (27)$$

or equivalently,  $\mathcal{O}(NL^2)$ .

### APPENDIX C: CRLB FOR THE DA-MLE

The CRLB for the CFO estimate is derived under the assumption that all the symbols transmitted within the burst, which are included in  $\mathbf{A}$ , are known. Based on the approach pursued in [18] for single-carrier transmission, the observation model we adopt is given by (5), i.e., it ignores the errors for nonzero CFO due to the filterbank being not exactly matched to the incoming waveform. However, the impact of these errors can be considered negligible for values of CFO up to a few percent of the signaling rate, as assumed throughout the paper. Bearing in mind that the probability density function  $p(\mathbf{z}; \nu)$  of the received samples  $\mathbf{z}$  in (5) for given  $\nu$  is

complex Gaussian with zero mean and covariance matrix  $\mathbf{C}_z(\nu)$ , the Fisher information results as [17]

$$I(\nu) = -\mathbf{E} \left\{ \frac{\partial^2 \ln p(\mathbf{z}; \nu)}{\partial \nu^2} \right\} = \text{tr} \left\{ \left[ \mathbf{C}_z^{-1}(\nu) \frac{\partial \mathbf{C}_z(\nu)}{\partial \nu} \right]^2 \right\}, \quad (28)$$

and correspondingly,  $\text{CRLB}(\nu) = I^{-1}(\nu)$ .

Putting the covariance matrix  $\mathbf{C}_z(\nu)$  in (6) into the form  $\mathbf{C}_z(\nu) = \Gamma(\nu)(\mathbf{A}\mathbf{C}_\varphi\mathbf{A}^H + \sigma^2\mathbf{I}_{LN})\Gamma(\nu)^H$ , its derivative with respect to  $\nu$  is found to be

$$\frac{\partial \mathbf{C}_z(\nu)}{\partial \nu} = j2\pi\Gamma(\nu) [\mathbf{H}(\mathbf{A}\mathbf{C}_\varphi\mathbf{A}^H + \sigma^2\mathbf{I}_{LN}) - (\mathbf{A}\mathbf{C}_\varphi\mathbf{A}^H + \sigma^2\mathbf{I}_{LN})\mathbf{H}] \Gamma(\nu)^H, \quad (29)$$

where the  $LN \times LN$  diagonal matrix  $\mathbf{H}$  is defined as  $\mathbf{H} \triangleq \text{diag} \{0, 1, \dots, L-1, \dots, 0, 1, \dots, L-1\}$ . Hence, substituting  $\mathbf{C}_z^{-1}(\nu) = \Gamma(\nu)(\mathbf{A}\mathbf{C}_\varphi\mathbf{A}^H + \sigma^2\mathbf{I}_{LN})^{-1}\Gamma(\nu)^H$  and (29) into (28) produces after some algebra the desired result

$$I(\nu) = 8\pi^2 \text{tr} \left\{ (\mathbf{C}_\varphi + \sigma^2\mathbf{I}_{LN})^{-1} \mathbf{H} (\mathbf{C}_\varphi + \sigma^2\mathbf{I}_{LN}) \mathbf{H} - \mathbf{H}^2 \right\}, \quad (30)$$

where  $\sigma^2$  is the inverse of the  $E_s/N_0$  ratio. Note that if  $\mathbf{C}_\varphi$  were a diagonal matrix, i.e., if the fading process were uncorrelated both in time and frequency, we would obtain  $I(\nu)=0$  and therefore  $\text{CRLB}(\nu) = \infty$ , thus meaning that the CFO estimation (as expected) would have no significance.

Finally, it can be of interest evaluating the asymptotic values of (30) in correspondence of  $\sigma \rightarrow \infty$  (low-SNR). After expanding

$$\left( \mathbf{I}_{LN} + \frac{1}{\sigma^2} \mathbf{C}_\varphi \right)^{-1} \quad (31)$$

into a matrix series under the assumption of  $\|\mathbf{C}_\varphi\|/\sigma^2 < 1$ , letting  $\sigma \rightarrow \infty$  yields

$$I_\infty(\nu) = 8\pi^2 \left( \frac{E_s}{N_0} \right)^2 \text{tr} \left\{ \mathbf{C}_\varphi^2 \mathbf{H}^2 - (\mathbf{C}_\varphi \mathbf{H})^2 \right\}, \quad (32)$$

whereas in the case of  $\sigma \rightarrow 0$  (high-SNR), we get

$$I_0(\nu) = 8\pi^2 \text{tr} \left\{ \mathbf{C}_\varphi^{-1} \mathbf{H} \mathbf{C}_\varphi \mathbf{H} - \mathbf{H}^2 \right\}, \quad (33)$$

which proves the existence of a floor in the CRLB due to the time-variance of the fading channel.

## REFERENCES

- [1] J. A. C. Bingham, "Multicarrier Modulation for Data Transmission: An Idea Whose Time Has Come," *IEEE Commun. Mag.*, vol. 28, no. 5, pp. 5–14, May 1990.
- [2] H. Sari, G. Karam and I. Jeanclaude, "Transmission Techniques for Digital Terrestrial TV Broadcasting," *IEEE Commun. Mag.*, vol. 33, pp. 100–109, Feb. 1995.
- [3] B. Crow, I. Widjaja, J. G. Kim, and P. Sakai, "IEEE 802.11 Wireless Local Area Networks," *IEEE Commun. Mag.*, vol. 35, pp. 116–126, Sept. 1997.
- [4] C. Eklund, R. B. Marks, K. L. Stanwood, and S. Wang, "IEEE Standard 802.16: A Technical Overview of the WirelessMAN Air Interface for Broadband Wireless Access," *IEEE Commun. Mag.*, vol. 40, no. 6, pp. 98–107, June 2002.
- [5] D. Astély, E. Dahlman, A. Furuskär, Y. Jading, M. Lindström, and S. Parkvall, "LTE: The Evolution of Mobile Broadband," *IEEE Commun. Mag.*, vol. 47, no. 4, pp. 44–51, April 2009.
- [6] ETSI EN 301 958, "Digital Video Broadcasting (DVB): Interaction Channel for Digital Terrestrial Television (RCT) Incorporating Multiple Access OFDM," Mar. 2002.
- [7] ETSI TS 300 392-2 V 3.1.1, "Terrestrial Trunked Radio (TETRA): TETRA Enhanced Data Service (TEDS), Air Interface Specification," Sept. 2006.
- [8] M. Nouri, V. Lottici, R. Reggiannini, D. Ball, and M. Rayne, "TEDS: A High Speed Digital Mobile Communication Air Interface for Professional Users," *IEEE Veh. Technol. Mag.*, vol. 1, no. 4, pp. 32–42, Dec. 2006.
- [9] M. Bellanger, G. Bonnerot, and M. Coudreuse, "Digital Filtering by Polyphase Network: Application to Sample-Rate Alteration and Filter Banks," *IEEE Trans. on Acoust., Speech, Signal Process.*, vol. 24, no. 2, pp. 109–114, Apr. 1976.
- [10] G. Cherubini, E. Eleftheriou and S. Ölçer, and J. Cioffi, "Filter Bank Modulation Techniques for Very High-Speed Digital Subscriber Lines," *IEEE Commun. Mag.*, vol. 38, pp. 98–104, May 2000.
- [11] S. D. Sandberg and M. A. Tzannes, "Overlapped Discrete Multitone Modulation for High Speed Copper Wire Communications," *IEEE J. Select. Areas Commun.*, vol. 13, no. 9, pp. 1571–1585, Dec. 1995.
- [12] P. Siohan, C. Siclet, and N. Lacaille, "Analysis and Design of OFDM/OQAM Systems based on Filterbank Theory," *IEEE Trans. on Signal Process.*, vol. 50, no. 5, pp. 1170–1183, May 2002.
- [13] V. Lottici, R. Reggiannini, and M. Carta, "Pilot-Aided Carrier Frequency Estimation for Filter-Bank Multicarrier Wireless Communications on Doubly-Selective Channels," *IEEE Trans. on Signal Process.*, vol. 58, no. 5, pp. 2783–2794, May 2010.
- [14] T. Fusco, A. Petrella, and M. Tanda, "Data-Aided Symbol Timing and CFO Synchronization for Filter Bank Multicarrier Systems," *IEEE Trans. on Wireless Commun.*, vol. 8, no. 5, pp. 2705–2715, May 2009.
- [15] V. Lottici, M. Luise, C. Saccomando, and F. Spalla, "Blind Carrier Frequency Tracking for Filterbank Multicarrier Wireless Communications," *IEEE Trans. on Commun.*, vol. 53, no. 10, pp. 1762–1772, Oct. 2005.
- [16] T. Fusco, A. Petrella, and M. Tanda, "Blind CFO Estimation for Noncritically Sampled FMT Systems," *IEEE Trans. on Signal Process.*, vol. 56, no. 6, pp. 2603–2608, June 2008.
- [17] S. M. Kay, *Fundamentals of Statistical Signal Processing: Estimation Theory*. Englewood Cliffs, NJ: Prentice-Hall, 1993.
- [18] W.-Y. Kuo and M. P. Fitz, "Frequency Offset Compensation of Pilot Symbol Assisted Modulation in Frequency Flat Fading," *IEEE Trans. on Commun.*, vol. 45, no. 11, pp. 1412–1416, Nov. 1997.

PA-MLE	$\mathcal{O}(N_\nu \chi^2 N^2 L^2)$
CMLE	$\mathcal{O}(N^2 L^2)$
LC-CMLE	$\mathcal{O}(NL^2)$

TABLE I

COMPUTATIONAL COMPLEXITY ORDER

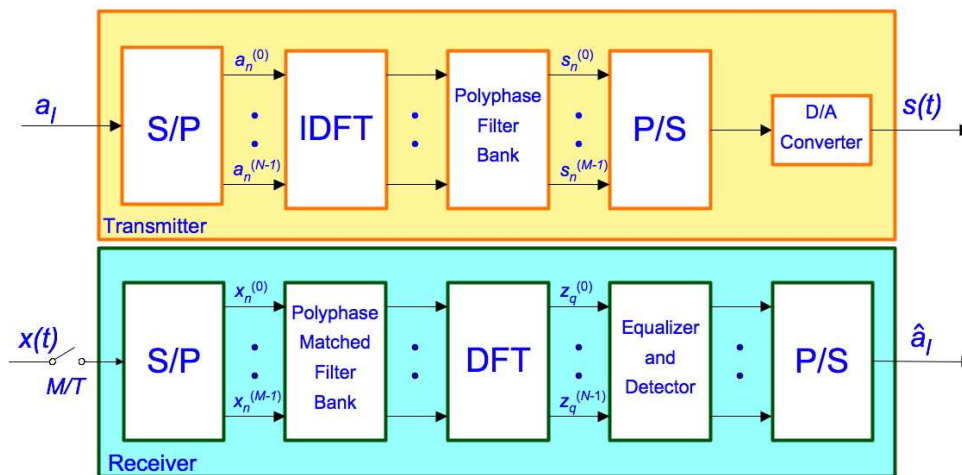


Fig. 1. FMT transmitter and receiver.

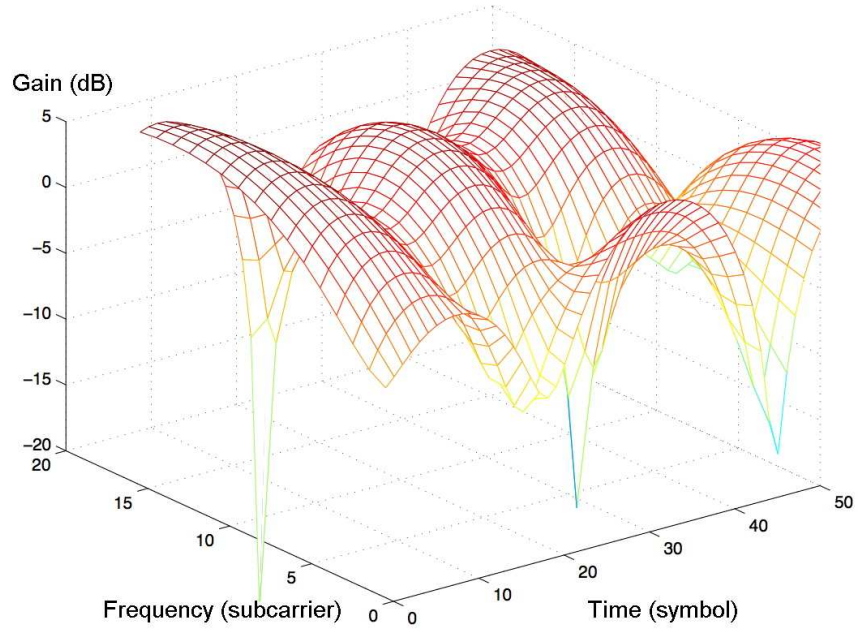


Fig. 2. A snapshot of the time-frequency fading process on fast-fading channel for  $N = 16$  and  $L = 51$ .

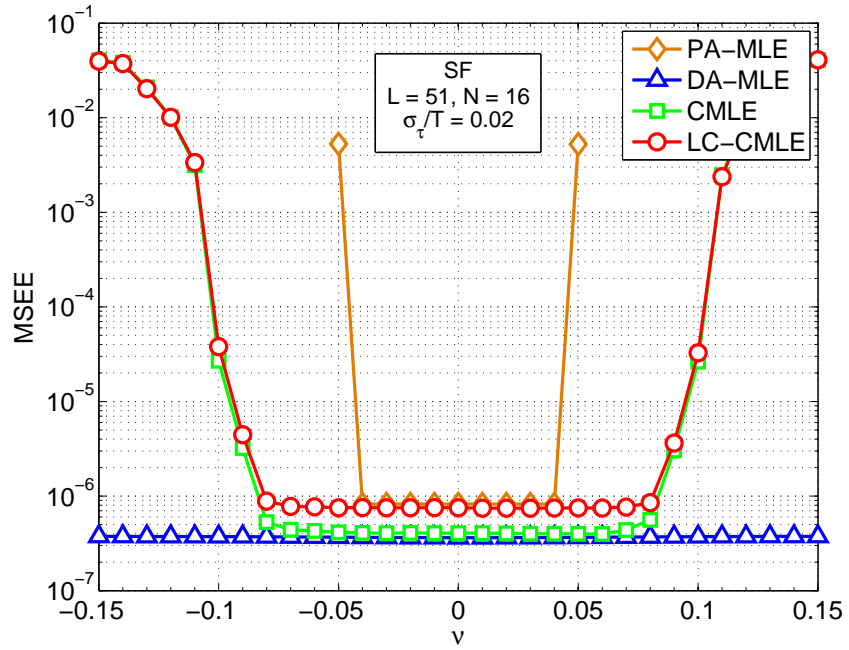


Fig. 3. Acquisition range on slow-fading channel at  $E_s/N_0 = 30$  dB and  $N = 16$ .

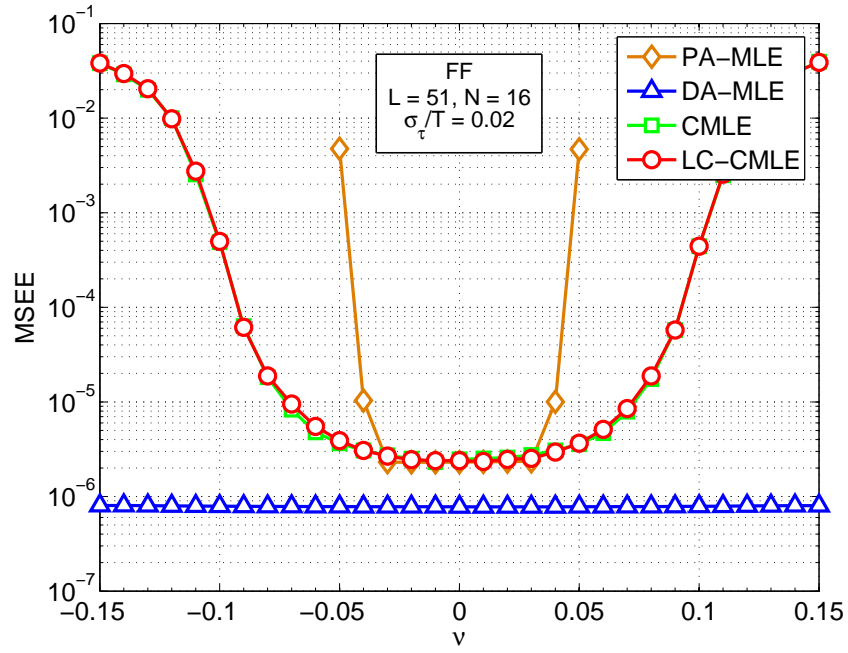


Fig. 4. Acquisition range on fast-fading channel at  $E_s/N_0 = 30$  dB and  $N = 16$ .

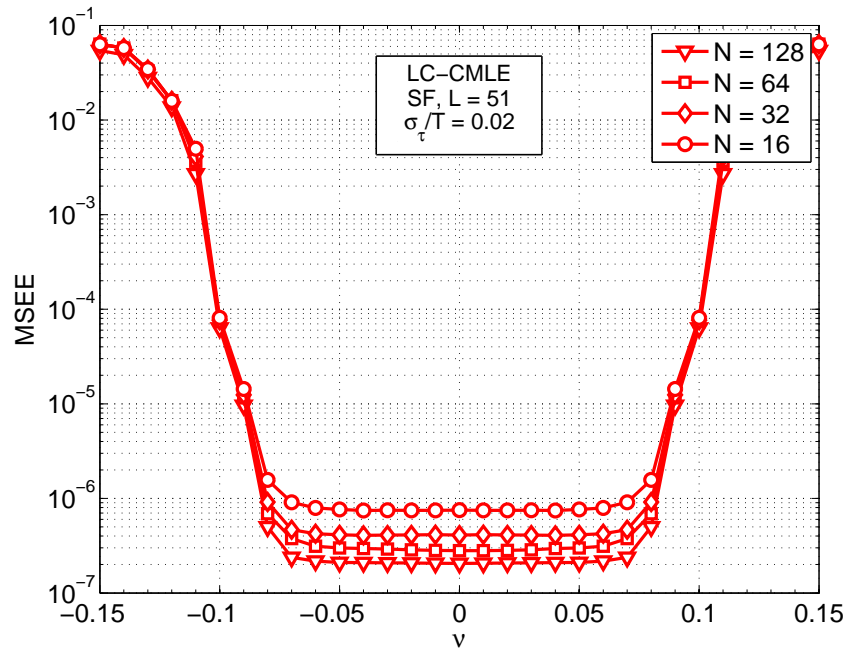


Fig. 5. Acquisition range of the LC-CMLE on slow-fading channel at  $E_s/N_0 = 30$  dB and  $N = 16, 32, 64, 128$ .

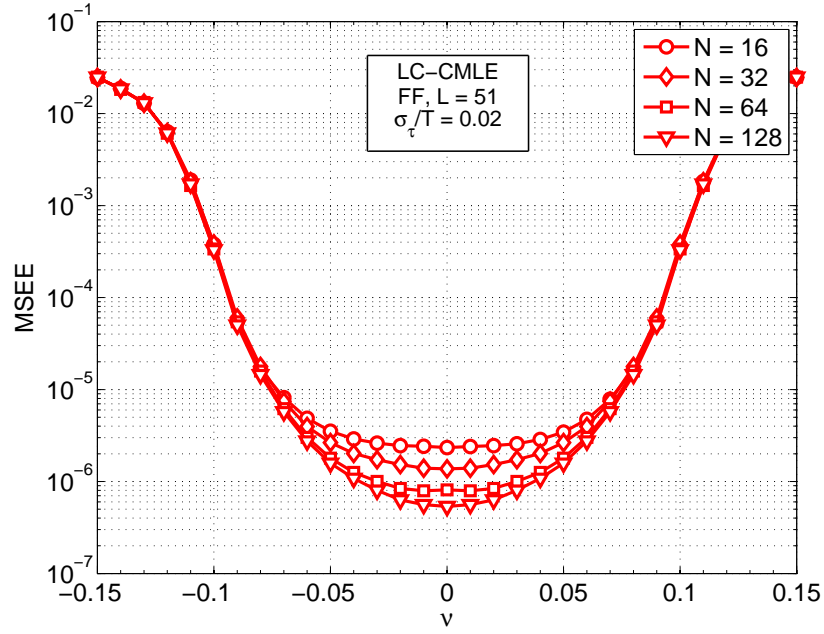


Fig. 6. Acquisition range of the LC-CMLE on fast-fading channel at  $E_s/N_0 = 30$  dB and  $N = 16, 32, 64, 128$ .

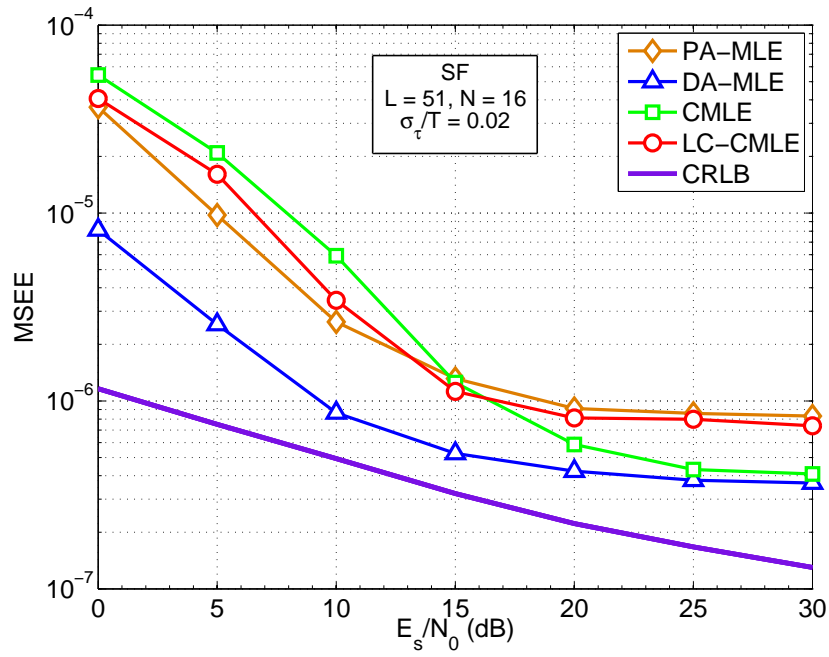


Fig. 7. MSEE versus  $E_s/N_0$  on slow-fading channel for  $\nu = 0$ .

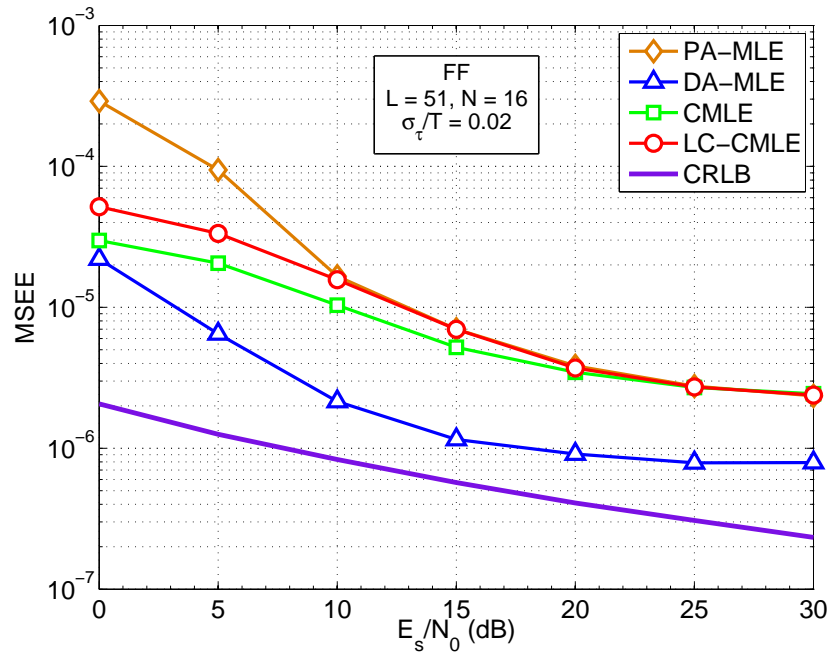


Fig. 8. MSEE versus  $E_s/N_0$  on fast-fading channel for  $\nu = 0$ .